Semiquantitative Parameters in PSMA-Targeted PET Imaging with ^{18}F-DCFPyL: Variability in Normal-Organ Uptake

Xin Li[1,2], Steven P. Rowe[1], Jeffrey P. Leal[1], Michael A. Gorin[3], Mohamad E. Allaf[3], Ashley E. Ross[3], Kenneth J. Pienta[3,4], Martin A. Lodge[1], and Martin G. Pomper[1]

[1]Russell H. Morgan Department of Radiology and Radiological Science, Johns Hopkins University School of Medicine, Baltimore, Maryland; [2]Department of Radiology, Shandong Provincial Hospital, Shandong University, Jinan City, Shandong Province, China; [3]James Buchanan Brady Urological Institute and Department of Urology, Johns Hopkins University School of Medicine, Baltimore, Maryland; and [4]Department of Medical Oncology, Johns Hopkins University School of Medicine, Baltimore, Maryland

^{18}F-DCFPyL is a small-molecule inhibitor of the prostate-specific membrane antigen that has shown promise for evaluation of primary and metastatic prostate cancer using PET. Measuring the variability in normal-organ uptake of ^{18}F-DCFPyL is necessary to understand its biodistribution, aid image interpretation, judge the reliability of scan quantification, and provide a basis for therapeutic monitoring. **Methods:** Sixty-five consecutive ^{18}F-DCFPyL PET/CT scans from 64 patients with a history of prostate cancer were analyzed. Volumes of interest were defined for the lacrimal glands, major salivary glands, liver, spleen, and both kidneys. The mean SUV normalized to body mass or to lean body mass (SUL) was calculated for each volume of interest. The average SUV across all scans, the SD, and the coefficient of variation (COV) for each organ were calculated. The same parameters were also derived for a 3-cm sphere drawn in the center of the right lobe of the liver. **Results:** The average SUV_{mean} for all selected organs measured was 6.6 ± 1.8 for the right lacrimal gland, 6.4 ± 1.8 for the left lacrimal gland, 9.1 ± 2.0 for the right parotid gland, 9.0 ± 2.1 for the left parotid gland, 9.6 ± 2.3 for the right submandibular gland, 9.4 ± 2.2 for the left submandibular gland, 5.0 ± 0.7 for the whole liver, 5.1 ± 0.7 for a 3-cm sphere in the liver, 4.0 ± 1.5 for the spleen, 20.1 ± 4.6 for the right kidney, and 19.4 ± 4.5 for the left kidney. SUL_{mean} was lower overall, although demonstrating similar trends. The COV of SUV_{mean} and SUL_{mean} was lower in the liver (13.8% and 14.5%, respectively) than in any other organ and was less than the comparable COV for ^{18}F-FDG PET. The COV of SUV_{mean} and SUL_{mean} in the 3-cm sphere in the liver was also low and similar to the variability in the whole liver (14.2% and 14.7%, respectively). **Conclusion:** ^{18}F-DCFPyL uptake in normal liver demonstrates less variability than in other ^{18}F-DCFPyL–avid organs, and its variability is less than the reported variability of ^{18}F-FDG in liver. Variability was slightly less for SUV_{mean} than for SUL_{mean}, suggesting that SUV_{mean} may be the preferable parameter for quantification of images obtained with ^{18}F-DCFPyL.

Key Words: prostate-specific membrane antigen; positron emission tomography; molecular imaging; SUV; prostate cancer

J Nucl Med 2017; 58:942–946
DOI: 10.2967/jnumed.116.179739

Prostate-specific membrane antigen (PSMA) is a human transmembrane protein that is highly expressed in prostate cancer, and the degree of expression correlates positively with tumor aggression, metastatic disease, and recurrence (*1–3*). Several reports have suggested that PSMA-targeted PET imaging has utility in prostate cancer (*4–11*). Many of these have been retrospective studies that have used ^{68}Ga-labeled PSMA ligands such as ^{68}Ga-PSMA-HBED-CC (*4–7*). We have focused on ^{18}F-labeled radiotracers for PSMA-targeted imaging (*8–12*) given the improved prospects for centralized radiotracer production and the potential for better image quality (*13*). We developed 2-(3-(1carboxy-5-(6-[^{18}F]fluoro-pyridine-3-carbonyl)amino]-pentyl)-ureido)-pentanedioic acid (^{18}F-DCFPyL) as a second-generation fluorinated PSMA-targeted PET radiotracer to improve the tissue distribution of our first-generation agent (*12,14*).

PET/CT imaging of cancer is important in assessing tumor response or progression during or after therapy. ^{18}F-FDG PET/CT, in particular, has emerged as a useful approach to the assessment of metabolic response in a variety of tumors, partly on the basis of its ability to quantify radiotracer uptake within tumors and quantitatively determine response to therapy (*15–18*). These characteristics of PET offer significant advantages over anatomic imaging, in which size and morphologic changes must be used to judge the presence or absence of disease and response to therapy.

^{18}F-DCFPyL is a new clinical radiotracer that has initially shown promise in identifying lesions caused by prostate cancer and may be an alternative approach for therapeutic monitoring (*10,11,19*). However, before embarking on studies to assess the capacity for such monitoring, the intrinsic variability of ^{18}F-DCFPyL uptake in normal organs must be understood. Any change in tumor uptake on serial quantitative studies can be assessed only in the context of the known intrinsic variability of the imaging test (*20*).

The primary aim of this study was to initially characterize the between-patient variability in normal-organ uptake in patients with prostate cancer undergoing^{18}FDCFPyL PET/CT. Characterization of variability with ^{18}F-DCFPyL may increase our understanding of other PSMA-targeted radiotracers such as those radiolabeled with ^{68}Ga or other radioisotopes.

A secondary aim of this work was to investigate whether, for ^{18}F-DCFPyL, it would be preferable to use SUV corrected for body mass or for lean body mass (i.e., SUL). Previous work has demonstrated that SUV showed a positive correlation with body mass in ^{18}F-FDG PET scans (*21,22*). Many centers use SUL for ^{18}F-FDG

Received Jun. 14, 2016; revision accepted Nov. 17, 2016.
For correspondence or reprints contact: Martin G. Pomper, Johns Hopkins Medical School, Cancer Research Building 2, Room 492 1550 Orleans St., Baltimore, MD 21231.
E-mail: mpomper@jhmi.edu
Published online Dec. 8, 2016.

PET so that uptake is independent of patient mass (*23*). The question of whether to use SUV or SUL has not been specifically addressed for PSMA-targeted agents such as ^{18}F-DCFPyL.

MATERIALS AND METHODS

Patients

We retrospectively reviewed 65 consecutive ^{18}F-DCFPyL PET/CT scans acquired between May 2014 and November 2015 from 64 patients with a history of prostate cancer. The mean age of the patients was 63.8 y (range, 45–88 y). Fifty-four patients (84.4%) were white, 8 (12.5%) were black, and 2 (3.1%) were of Asian ancestry. All patients were imaged with protocols approved by the local Institutional Review Board, and all gave written informed consent before undergoing imaging. The patients were enrolled in imaging trials for preoperative staging (12, 18.8%), to delineate sites of disease in the context of recurrence after radical retropubic prostatectomy (44, 68.8%), or to evaluate metastatic disease (9, 14.0%). One patient had a past history of splenectomy, but there were no other major abdominal organ resections in this patient cohort.

^{18}F-DCFPyL PET/CT Imaging

^{18}F-DCFPyL was produced using a dual-run ^{18}F-FDG synthesis module according to a modification of a synthetic route previously described by Chen et al. (*12*). Fifty-nine of the PET scans were performed on a Discovery RX PET/CT scanner (GE Healthcare), and the remaining 6 scans were acquired on a Biograph mCT scanner (Siemens Healthcare). Both devices were operated in 3-dimensional emission acquisition mode and used CT for attenuation correction.

The patients fasted for 4–6 h before injection of ^{18}F-DCFPyL. Approximately 1 h after intravenous injection of ^{18}F-DCFPyL (≤333 MBq [≤9 mCi]), PET images of the supine patients were acquired over 6–8 bed positions (depending on the scanner used and the patient height) from the mid thighs to the skull vertex. PET and CT acquisition parameters were similar between the two scanners, although some differences are noted in Supplemental Table 1 (supplemental materials are available at http://jnm.snmjournals.org). Routine quality assurance phantoms confirmed that PET images from the two scanners were quantitatively comparable, and quality evaluations of clinical ^{18}F-FDG studies indicated no statistically significant difference (Student t test, $P = 0.39$) between the mean liver SULs obtained from the two systems.

Image Analysis

PET images were analyzed using XD3 Software (Mirada Medical), which allowed review of PET, CT, and fused-image data. Volumes of interest (VOIs) were manually drawn over the entire organ volume using the best visual approximation of the organ edge as has previously been described (*20*). Given the biodistribution of ^{18}F-DCFPyL, these VOIs included both lacrimal glands, all 4 major salivary glands, the liver, the spleen, and both kidneys for all patients. Representative VOIs displayed on a maximum-intensity-projection image are shown in Figure 1. The CT images were available only for localization and were not used to guide delineation of the VOIs.

Between-patient variability was assessed for each organ and SUV definition (SUV or SUL) by taking the average, SD, and coefficient of variation (COV) across all patients. The same parameters were also derived for a 3-cm sphere drawn in the center of the nondiseased right hepatic lobe of the liver, a potentially more convenient VOI for clinical application.

Statistical Analysis

Data are presented as mean ± SD and the COV for each organ. The independent-samples t test was used to compare the difference in uptake values between the 3-cm-sphere VOI and the whole-liver VOI. The relationship of SUV_{mean} and SUL_{mean} to patient body weight was assessed by the Pearson correlation coefficient using SPSS software (version 17.0).

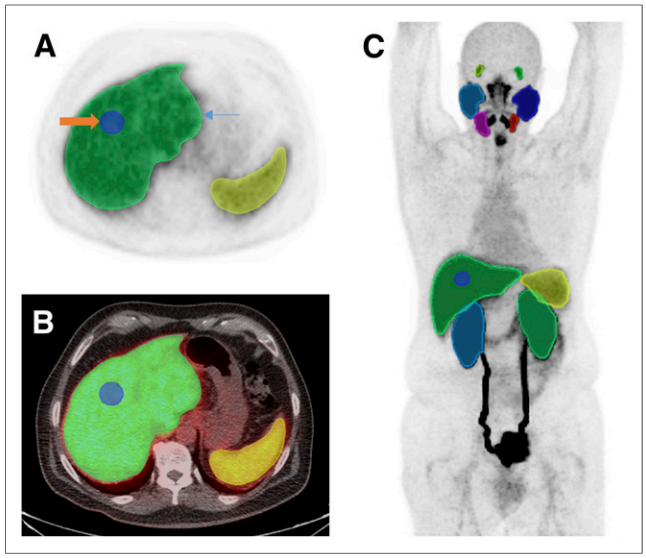

FIGURE 1. (A) axial ^{18}F-DCFPyL PET image through upper abdomen including liver and spleen showing whole-organ VOI (blue arrow) and 3-cm-sphere VOI in right lobe of liver (orange arrow). (B) Corresponding axial fused ^{18}F-DCFPyL PET/CT images. (C) Representative organ VOIs displayed on maximum-intensity-projection image.

RESULTS

Sixty-three of 64 patients (98.4%) had visually normal biodistribution findings. One patient's biodistribution differed only in lacking a spleen, consistent with a history of prior splenectomy. The calculated averages and SDs for SUV_{mean} and SUL_{mean} for each organ are displayed in Table 1. As expected from visual assessment, SUV_{mean} and SUL_{mean} were higher in the kidneys than in any other examined organ (SUV_{mean}, 20.1 ± 4.6 on the right and 19.4 ± 4.5 on the left; SUL_{mean}, 14.8 ± 3.4 on the right and 14.3 ± 3.3 on the left). The major salivary glands had, on average, higher uptake values than any other organ except for the kidneys, with SUV_{mean} ranging from 9.0 ± 2.1 to 9.6 ± 2.3 and SUL_{mean} ranging from 6.7 ± 1.7 to 7.1 ± 1.6. The lacrimal glands also demonstrated high average uptake, with an SUV_{mean} of 6.6 ± 1.8 on the right and 6.4 ± 1.8 on the left and an SUL_{mean} of 4.9 ± 1.3 on the right and 4.8 ± 1.3 on the left. The highly similar values obtained between the paired organs suggests that the images are spatially reliable and that there were no significant errors in the manner in which the VOIs were manually rendered.

Regarding the 2 unpaired organs in this study, the liver demonstrated overall higher uptake than the spleen. SUV_{mean} for the liver was 5.0 ± 0.7, and SUL_{mean} was 3.8 ± 0.5. SUV_{mean} for the spleen was 4.0 ± 1.5, and SUL_{mean} was 2.9 ± 1.1 (Fig. 2).

The calculated COVs across all patients for SUV_{mean} and SUL_{mean} are included in Table 2. Variabilities between paired organs are similar regardless of the use of SUV or SUL (e.g., 26.9% for the right lacrimal gland and 27.6% for the left lacrimal gland when using SUV_{mean} and 26.3% for the right lacrimal gland and 26.5% for the left lacrimal gland when using SUL_{mean}). The lowest variability of any of the studied organs was in the liver, where the COV was 13.8% for SUV_{mean} and 14.5% for SUL_{mean}, whereas the highest variability was in the spleen (38.7% with SUV_{mean} and 38.8% for SUL_{mean}). For reference, the COV of the liver with ^{18}F-FDG PET has been reported to be 21.0%–23.1%

TABLE 1
SUV_{mean} and SUL_{mean} for Each Organ Across All Patients

Organ	SUV_{mean}	SUL_{mean}
Right lacrimal gland	6.6 ± 1.8	4.9 ± 1.3
Left lacrimal gland	6.4 ± 1.8	4.8 ± 1.3
Right parotid gland	9.1 ± 2.0	6.8 ± 1.6
Left parotid gland	9.0 ± 2.1	6.7 ± 1.7
Right submandibular gland	9.6 ± 2.3	7.1 ± 1.6
Left submandibular gland	9.4 ± 2.2	6.9 ± 1.6
Liver	5.0 ± 0.7	3.8 ± 0.5
Spleen	4.0 ± 1.5	2.9 ± 1.1
Right kidney	20.1 ± 4.6	14.8 ± 3.4
Left kidney	19.4 ± 4.5	14.3 ± 3.3

Data are average and SD of uptake parameters.

TABLE 2
COVs for SUV_{mean} and SUL_{mean} for Each Organ Across All Patients

Organ	SUV_{mean}	SUL_{mean}
Right lacrimal gland	26.9%	26.3%
Left lacrimal gland	27.6%	26.5%
Right parotid gland	22.0%	23.5%
Left parotid gland	23.3%	24.5%
Right submandibular gland	24.3%	23.3%
Left submandibular gland	23.5%	23.7%
Liver	13.8%	14.5%
Spleen	38.7%	38.8%
Right kidney	23.1%	22.6%
Left kidney	23.2%	22.7%

using SUL_{mean} (*24*). Only 1 of the 64 patients included in this study was imaged at more than a single time point, so no data are available on the relative roles of intrapatient (test–retest) versus interpatient variability.

Although the whole-organ VOIs would likely be the most reliable means of determining average uptake in normal organs, drawing such VOIs is time-consuming and unlikely to be undertaken in the context of a busy clinical workflow. We investigated the ability of a simple 3-cm-diameter sphere placed within visually normal liver parenchyma (Fig. 1) to represent the activity in the whole-organ liver VOI. SUV_{mean}, SUL_{mean}, and COV for the 3-cm-sphere VOIs were found to be similar to the whole-organ VOI uptake values (Table 3). The average SUV_{mean} of the 3-cm spheres in the liver was 5.1 ± 0.7 (compared with 5.0 ± 0.7), whereas the average SUL_{mean} in the 3-cm spheres was 3.8 ± 0.6 (compared with 3.8 ± 0.5). We used independent-samples *t* testing and found no significant difference between 3-cm-sphere and whole-liver VOIs (SUL_{mean}, $t = -0.37$, $P = 0.71$; SUV_{mean}, $t = -0.40$, $P = 0.69$). The COVs in the 3-cm-sphere VOIs (14.2% using SUV_{mean} and 14.7% using SUL_{mean}) were similar to those of the whole-liver VOIs (13.8% using SUV_{mean} and 14.5% using SUL_{mean}).

The average body mass of the 64 male patients was 88.5 ± 12.8 kg (range, 57.0–136.0 kg). That relatively wide range of patient masses allowed us to investigate for the presence of any correlation between body mass and uptake parameters. Because the variability in the liver across all scans was less than that in any other included organ, we plotted SUV_{mean} in the liver against body mass and found that there was no significant correlation between them (Pearson analysis: $r = 0.195$, $P = 0.119$; Fig. 3). SUL_{mean} in the liver was also tested for a correlation with body mass, and again, no significant correlation was found ($r = -0.190$, $P = 0.130$; Fig. 3).

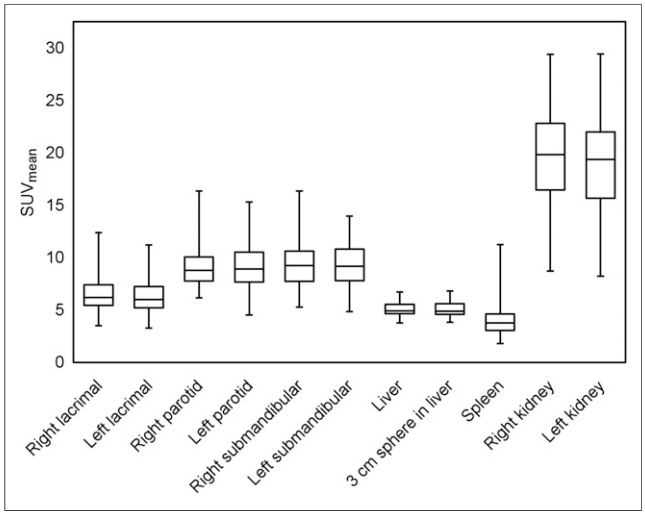

FIGURE 2. Box-and-whisker chart shows uptake of ^{18}F-DCFPyL in different organs. SUV_{mean} in kidneys was highest of any examined organs, followed by salivary and lacrimal glands. Lowest uptake was in spleen, that in liver being slightly higher.

DISCUSSION

As PSMA-targeted radiotracers continue to be used in the detection of prostate cancer lesions in a wide variety of clinical settings, it will become increasingly important to understand the quantitative and semiquantitative aspects of these new agents. When PSMA-guided focal therapies such as stereotactic body radiation gain further clinical acceptance, and as PSMA-based endoradiotherapy continues to be used in more locations for widely metastatic disease (*25,26*), the need to quantitatively evaluate tumors and their response to therapy will increase.

PSMA is also consistently and abundantly expressed on the neovascular endothelium in a wide variety of human solid tumors (*27–30*), suggesting that agents such as ^{18}F-DCFPyL may be used as general radiotracers for oncologic imaging. This has recently been demonstrated for metastatic clear cell renal cell carcinoma (*11,12,31*). For these reasons, we addressed the semiquantitative aspects of imaging with ^{18}F-DCFPyL as they relate to normal-organ variability.

The levels of variation in normal organs on ^{18}F-DCFPyL PET scans must be known so that changes in uptake in malignant lesions can be confidently attributed to a change in disease or therapeutic response as opposed to the intrinsic variability of the scan. In ^{18}F-FDG PET studies, the quantitative framework of PERCIST 1.0 required a 30% decline in SUV for a tumor to be considered to have a true response (*16*). Liver was chosen as the basis of quantitative reliability in PET images given its moderate level of ^{18}F-FDG uptake

TABLE 3
SUV_{mean}, SUL_{mean}, and COV for 3-Centimeter-Sphere and Whole-Liver VOIs

Parameter	VOI	
	3-cm sphere	Whole liver
SUV_{mean}	5.1 ± 0.7	5.0 ± 0.7
SUL_{mean}	3.8 ± 0.6	3.8 ± 0.5
SUV_{mean} COV	14.2%	13.8%
SUL_{mean} COV	14.7%	14.5%

in normal parenchyma and the low variability in uptake relative to other organs (*16*). In a metaanalysis on the repeatability of ^{18}F-FDG uptake measurements in tumors, a minimal relative change of 20% in combination with a 1.2-unit change in SUV_{mean} was presumed to represent a biologic change (*32*).

Here, we assessed the variability of ^{18}F-DCFPyL uptake in a variety of solid organs (salivary glands, lacrimal glands, liver, spleen, and kidneys). Analogous to ^{18}F-FDG, uptake in the normal liver was moderate and appeared visually homogeneous. Uptake in the liver had the lowest variability of any of the organs included in this study (COV of 13.8% when using SUV_{mean} and 14.5% when using SUL_{mean}, both of which are lower than the 21%–23% COVs previously reported for ^{18}F-FDG PET in liver (*24*)). These data imply that ^{18}F-DCFPyL PET images, and perhaps PSMA-targeted PET images in general, can be quantified reliably and possibly with higher fidelity than the corresponding ^{18}F-FDG images.

A spheric 3-cm-diameter VOI in the normal-liver parenchyma accurately represented uptake within the entire liver volume, with no significant difference in average uptake when either SUV_{mean} or SUL_{mean} was used ($P > 0.05$). This is an important consideration in the clinical translation of the principles of this study given the impracticality of delineating whole-organ VOIs during clinical workflow.

Uptake seen on PET scans is commonly normalized to body mass (SUV) or lean body mass (SUL). SUL is preferred by many centers over SUV for quantification in ^{18}F-FDG studies because there is a strong positive correlation between the blood SUV and body mass ($r = 0.705$, $P < 0.001$), but SUL has shown no correlation with body mass ($r = -0.010$, $P = 0.904$) (*23,33*). In the course of our evaluation of normal-organ uptake variability, we investigated both SUV and SUL for ^{18}F-DCFPyL. We calculated the correlation between both SUV_{mean} and SUL_{mean} and body mass for the liver, and the scatterplots showed no significant correlation ($r = 0.195$, $P = 0.119$, for SUV_{mean}; $r = -0.190$, $P = 0.130$, for SUL_{mean}). We concluded from these findings that both SUV_{mean} and SUL_{mean} can be used in the assessment of ^{18}F-DCFPyL uptake, although the lower normal-organ variability calculated with SUV_{mean} (COV 13.76% vs. COV 14.47% with SUL_{mean}) would argue that SUV should be used.

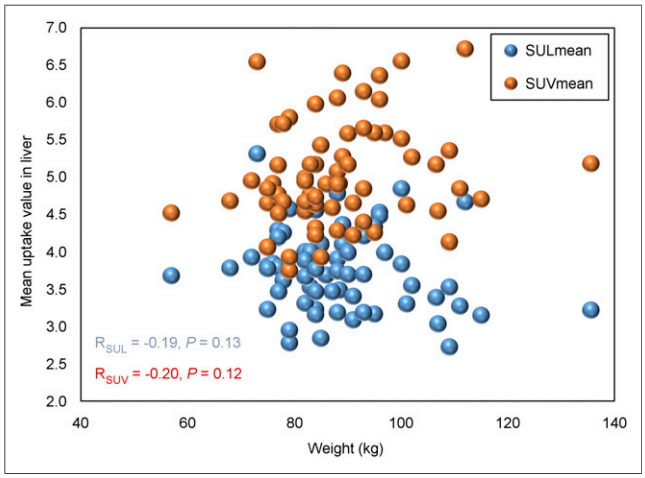

FIGURE 3. Scatterplots of SUV_{mean} and SUL_{mean} in liver against body mass. SUV_{mean} in liver had no significant correlation with mass based on Pearson analysis ($r = 0.195$, $P = 0.119$). There was also no significant correlation between SUL_{mean} in liver and body mass ($r = -0.19$, $P = 0.13$).

A prospective test–retest study that scans patients twice with ^{18}F-DCFPyL within a short period and without intervening therapy will ultimately be needed to assess the ground-state variability of ^{18}F-DCFPyL in normal organs and tumors and to continue to lay the groundwork for threshold cutoffs for determining response to therapy. Given the similarities in biodistribution between ^{18}F-DCFPyL and other PSMA-based radiotracers such as the ^{68}Ga-labeled agents (*4–7*), it is likely that quantitative and semiquantitative principles learned with one such radiotracer will apply broadly to other agents in this class. Even without dedicated test–retest studies, the data in this study suggest that semiquantitative analysis is both feasible and promising.

Potential limitations of this study include the possibility that partial-volume effects at the periphery of organs will degrade the reliability of average uptake measurements and increase variability, although we believe such effects are likely minimal given the similarity in both absolute uptake and variability between whole-liver VOIs and spheric VOIs in the middle of the liver parenchyma. Any partial-volume effects at the edge would likely be greatest for smaller organs such as the lacrimal glands. With regard to nearby organs, such as the liver and right kidney or the spleen and left kidney, these could cause some overlap in uptake that would be difficult to avoid when drawing whole-organ VOIs.

Furthermore, we included patients undergoing imaging for multiple indications and with a widely ranging amount of radiotracer-avid disease, potentially increasing the measured variability in normal-organ uptake through redistribution of radiotracer to sites of disease. Including such a breadth of patients, however, increases the generalizability of the findings, as the variability results described herein should be applicable to many different patients undergoing PSMA-targeted imaging.

We should also note that we have previously advocated imaging with ^{18}F-DCFPyL at 2 h after injection because of the possibility of identifying subtle lesions at a later time point as well as improving tumor-to-background ratios (*34*); however, for reasons of clinical expediency, we have generally imaged patients at 1 h after injection. Even greater stability in normal-organ uptake variation might be achievable at a later time point, but we have not specifically investigated this possibility.

CONCLUSION

Variability in normal-liver uptake was less for ^{18}F-DCFPyL than has been shown for ^{18}F-FDG. This finding implies that ^{18}F-DCFPyL PET images, and perhaps PSMA-targeted PET images in general, can be reliably quantified, laying the groundwork for future studies involving therapeutic monitoring. Neither SUV_{mean} nor SUL_{mean}

correlated significantly with body mass; however, the variability in liver uptake calculated from SUV_{mean} was marginally less than that calculated from SUL_{mean}, favoring adoption of SUV for ^{18}F-DCFPyL PSMA-targeted PET scans.

DISCLOSURE

This work was supported by the National Institutes of Health (grants CA134675 and CA183031) and by philanthropic funds provided to the James Buchanan Brady Urological Institute and Department of Urology. Martin G. Pomper is a coinventor on a U.S. patent covering ^{18}F-DCFPyL and as such is entitled to a portion of any licensing fees and royalties generated by this technology. This arrangement has been reviewed and approved by the Johns Hopkins University in accordance with its conflict-of-interest policies. No other potential conflict of interest relevant to this article was reported.

REFERENCES

1. Perner S, Hofer MD, Kim R, et al. Prostate-specific membrane antigen expression as a predictor of prostate cancer progression. *Hum Pathol.* 2007;38:696–701.
2. Haberkorn U, Eder M, Kopka K, et al. New strategies in prostate cancer: prostate-specific membrane antigen (PSMA) ligands for diagnosis and therapy. *Clin Cancer Res.* 2016;22:9–15.
3. Silver DA, Pellicer I, Fair WR, et al. Prostate-specific membrane antigen expression in normal and malignant human tissues. *Clin Cancer Res.* 1997;3:81–85.
4. Afshar-Oromieh A, Malcher A, Eder M, et al. PET imaging with a [^{68}Ga]gallium-labelled PSMA ligand for the diagnosis of prostate cancer: biodistribution in humans and first evaluation of tumour lesions. *Eur J Nucl Med Mol Imaging.* 2013;40:486–495.
5. Eiber M, Maurer T, Souvatzoglou M, et al. Evaluation of hybrid ^{68}Ga-PSMA ligand PET/CT in 248 patients with biochemical recurrence after radical prostatectomy. *J Nucl Med.* 2015;56:668–674.
6. Afshar-Oromieh A, Avtzi E, Giesel FL, et al. The diagnostic value of PET/CT imaging with the ^{68}Ga-labelled PSMA ligand HBED-CC in the diagnosis of recurrent prostate cancer. *Eur J Nucl Med Mol Imaging.* 2015;42:197–209.
7. Eder M, Neels O, Müller M, et al. Novel preclinical and radiopharmaceutical aspects of [^{68}Ga]Ga-PSMA-HBED-CC: a new PET tracer for imaging of prostate cancer. *Pharmaceuticals (Basel).* 2014;7:779–796.
8. Cho SY, Gage KL, Mease RC, et al. Biodistribution, tumor detection, and radiation dosimetry of ^{18}F-DCFBC, a low-molecular-weight inhibitor of prostate-specific membrane antigen, in patients with metastatic prostate cancer. *J Nucl Med.* 2012;53:1883–1891.
9. Rowe SP, Gage KL, Faraj SF, et al. ^{18}F-DCFBC PET/CT for PSMA-based detection and characterization of primary prostate cancer. *J Nucl Med.* 2015;56:1003–1010.
10. Rowe SP, Macura KJ, Ciarallo A, et al. Comparison of prostate-specific membrane antigen-based ^{18}F-DCFBC PET/CT to conventional imaging modalities for detection of hormone-naïve and castration-resistant metastatic prostate cancer. *J Nucl Med.* 2016;57:46–53.
11. Szabo Z, Mena E, Rowe SP, et al. Initial evaluation of [^{18}F]DCFPyL for prostate-specific membrane antigen (PSMA)-targeted PET imaging of prostate cancer. *Mol Imaging Biol.* 2015;17:565–574.
12. Chen Y, Pullambhatla M, Foss CA, et al. 2-(3-{1-carboxy-5-[(6-[^{18}F]fluoropyridine-3-carbonyl)-amino]-pentyl}-ureido)-pentanedioic acid, [^{18}F]DCFPyL, a PSMA-based PET imaging agent for prostate cancer. *Clin Cancer Res.* 2011;17:7645–7653.
13. Sanchez-Crespo A. Comparison of gallium-68 and fluorine-18 imaging characteristics in positron emission tomography. *Appl Radiat Isot.* 2013;76:55–62.
14. Chen Y, Foss CA, Byun Y, et al. Radiohalogenated prostate-specific membrane antigen (PSMA)-based ureas as imaging agents for prostate cancer. *J Med Chem.* 2008;51:7933–7943.
15. O JH, Lodge MA, Wahl RL. Practical PERCIST: a simplified guide to PET response criteria in solid tumors 1.0. *Radiology.* 2016;280:576–584.
16. Wahl RL, Jacene H, Kasamon Y, et al. From RECIST to PERCIST: evolving considerations for PET response criteria in solid tumors. *J Nucl Med.* 2009;50 (suppl 1):122S–150S.
17. Avril S, Muzic RF Jr, Plecha D, et al. ^{18}F-FDG PET/CT for monitoring of treatment response in breast cancer. *J Nucl Med.* 2016;57(suppl 1):34S–39S.
18. Sheikhbahaei S, Wray R, Young B, et al. ^{18}F-FDG-PET/CT therapy assessment of locally advanced pancreatic adenocarcinoma: impact on management and utilization of quantitative parameters for patient survival prediction. *Nucl Med Commun.* 2016;37:231–238.
19. Rowe SP, Mana-Ay M, Javadi MS. PSMA-based detection of prostate cancer bone lesions with ^{18}F-DCFPyL PET/CT: a sensitive alternative to ^{99m}Tc-MDP bone scan and Na^{18}F PET/CT? *Clin Genitourin Cancer.* 2016;14:e115–e118.
20. Rowe SP, Vicente E, Anizan N, et al. Repeatability of radiotracer uptake in normal abdominal organs with ^{111}In-pentetreotide quantitative SPECT/CT. *J Nucl Med.* 2015;56:985–988.
21. Batallés SM, Villavicencio RL, Quaranta A, et al. Variations of the hepatic SUV in relation to the body mass index in whole body PET-CT studies. *Rev Esp Med Nucl Imagen Mol.* 2013;32:26–32.
22. Kuhnert G, Boellaard R, Sterzer S, et al. Impact of PET/CT image reconstruction methods and liver uptake normalization strategies on quantitative image analysis. *Eur J Nucl Med Mol Imaging.* 2016;43:249–258.
23. Sugawara Y, Zasadny KR, Neuhoff AW, Wahl RL. Reevaluation of the standardized uptake value for FDG: variations with body weight and methods for correction. *Radiology.* 1999;213:521–525.
24. Viner M, Mercier G, Hao F, et al. Liver SULmean at FDG PET/CT: interreader agreement and impact of placement of volume of interest. *Radiology.* 2013; 267:596–601.
25. Kratochwil C, Giesel FL, Stefanova M, et al. PSMA-targeted radionuclide therapy of metastatic castration-resistant prostate cancer with ^{177}Lu-labeled PSMA-617. *J Nucl Med.* 2016;57:1170–1176.
26. Zechmann CM, Afshar-Oromieh A, Armor T, et al. Radiation dosimetry and first therapy results with a ^{124}I/^{131}I-labeled small molecule (MIP-1095) targeting PSMA for prostate cancer therapy. *Eur J Nucl Med Mol Imaging.* 2014; 41:1280–1292.
27. Chang SS, Reuter VE, Heston WD, et al. Five different anti-prostate-specific membrane antigen (PSMA) antibodies confirm PSMA expression in tumor associated neovasculature. *Cancer Res.* 1999;59:3192–3198.
28. Chang SS, O'Keefe DS, Bacich DJ, et al. Prostate-specific membrane antigen is produced in tumor-associated neovasculature. *Clin Cancer Res.* 1999;5:2674–2681.
29. Schülke N, Varlamova OA, Donovan GP, et al. The homodimer of prostate specific membrane antigen is a functional target for cancer therapy. *Proc Natl Acad Sci USA.* 2003;100:12590–12595.
30. Haffner MC, Kronberger IE, Ross JS, et al. Prostate-specific membrane antigen expression in the neovasculature of gastric and colorectal cancers. *Hum Pathol.* 2009;40:1754–1761.
31. Rowe SP, Gorin MA, Hammers HJ, et al. Imaging of metastatic clear cell renal cell carcinoma with PSMA-targeted ^{18}F-DCFPyL PET/CT. *Ann Nucl Med.* 2015;29:877–882.
32. de Langen AJ, Vincent A, Velasquez LM, et al. Repeatability of ^{18}F-FDG uptake measurements in tumors: a meta-analysis. *J Nucl Med.* 2012;53:701–708.
33. Zasadny KR, Wahl RL. Standardized uptake values of normal tissues at PET with 2-[fluorine-18]-fluoro-2-deoxy-D-glucose: variations with body weight and a method for correction. *Radiology.* 1993;189:847–850.
34. Rowe SP, Macura KJ, Mena E, et al. PSMA-based [^{18}F]DCFPyL PET/CT is superior to conventional imaging for lesion detection in patients with metastatic prostate cancer. *Mol Imaging Biol.* 2016;18:411–419.